Chemical Science

ROYAL SOCIETY OF CHEMISTRY

PERSPECTIVE

View Article Online
View Journal | View Issue

Cite this: *Chem. Sci.*, 2024, **15**, 4222

All publication charges for this article have been paid for by the Royal Society of Chemistry

Recent progress in ion-regulated organic room-temperature phosphorescence

Wenbo Dai,[ab] Yitian Jiang,[a] Yunxiang Lei,[a] Xiaobo Huang,[a] Peng Sun,[c] Jianbing Shi,[b] Bin Tong,[b] Dongpeng Yan,*[d] Zhengxu Cai*[b] and Yuping Dong[b]

Organic room-temperature phosphorescence (RTP) materials have attracted considerable attention for their extended afterglow at ambient conditions, eco-friendliness, and wide-ranging applications in bio-imaging, data storage, security inks, and emergency illumination. Significant advancements have been achieved in recent years in developing highly efficient RTP materials by manipulating the intermolecular interactions. In this perspective, we have summarized recent advances in ion-regulated organic RTP materials based on the roles and interactions of ions, including the ion–π interactions, electrostatic interactions, and coordinate interactions. Subsequently, the current challenges and prospects of utilizing ionic interactions for inducing and modulating the phosphorescent properties are presented. It is anticipated that this perspective will provide basic guidelines for fabricating novel ionic RTP materials and further extend their application potential.

Received 25th December 2023
Accepted 21st February 2024

DOI: 10.1039/d3sc06931a

rsc.li/chemical-science

Introduction

Organic room-temperature phosphorescence (RTP), that is persistent luminescence or afterglow emission,[1–4] has drawn extensive attention in optical and optoelectronic fields such as data storage,[5–7] sensors,[8–11] and bioimaging,[12–19] owing to its long emission lifetime, large Stokes shifts, and abundant excited states.[20–22] Currently, two critical factors are considered indispensable to achieve RTP with high efficiency (Φ_P) and long lifetime (τ_P).[23–25] As shown in Scheme 1a, one of the factors is the facilitation of the singlet-to-triplet intersystem crossing (ISC) to populate the triplet state (Φ_{ISC}), and the other is the maximum inhibition of the non-radiative relaxation pathways (k_{nr}) and oxygen quenching of the excited states (k_q).[26–29] In the past decades, several effective strategies, such as crystal engineering,[30–33] H-aggregation,[34–36] supramolecular assembly,[37–39] polymerization,[12,40–42] host–guest doping[43–52] and so on,[53–55] have been proposed to develop highly efficient RTP materials. Notably, numerous efforts have been devoted to suppressing the non-radiative transitions by covalent bonding, hydrogen bonding, and van der Waals forces for the realization of long-lived efficiency phosphorescence.[28]

During the last a few years, many classes of RTP materials particularly organic or metal ions substances have been developed for long lifetime and high quantum yields.[56–60] As a novel class of photo-functional materials, ionic systems, compared to ordinary organic neutral systems, could be promising RTP candidates to achieve the aforementioned critical factors due to the following advantages. Firstly, ionic systems could introduce modifiable metal centers and halogen units, enabling the manipulation of the heavy-atom effect to augment spin–orbit coupling (SOC) and, consequently, facilitating the ISC process.[61–63] Secondly, the rigid environment established through the ionic or coordinate bonding in the ionic systems could increase molecular conformational rigidity, which could effectively inhibit the non-radiative transitions of the triplet excitons.[64–66] Finally, the excited states of ionic systems could be more easily manipulated by modulating the ion species and intermolecular interactions, thereby endowing ionic RTP materials with abundant photophysical characteristics.[67–69] Considering these advantages, ionic systems serve as an essential and promising platform for creating novel RTP materials and have attracted wide attention. Despite the large scientific advances in the development of ionic RTP materials, systematic summary for the emission mechanism and rational design strategy still need to be made available.

Herein, we aim to elucidate the significant impact of the different types of ions and intermolecular interactions in ionic systems for achieving and regulating high-performance RTP materials. More specifically, by analyzing the functional role of

[a]*College of Chemistry and Materials Engineering, Wenzhou University, Wenzhou, China*

[b]*Beijing Key Laboratory of Construction Tailorable Advanced Functional Materials and Green Applications, School of Materials Science and Engineering, Beijing Institute of Technology, Beijing, China. E-mail: caizx@bit.edu.cn*

[c]*Advanced Research Institute of Multidisciplinary Sciences, Beijing Institute of Technology, Beijing, China*

[d]*Beijing Key Laboratory of Energy Conversion and Storage Materials, Key Laboratory of Radiopharmaceuticals, Ministry of Education, College of Chemistry, Beijing Normal University, Beijing, China. E-mail: yandp@bnu.edu.cn*

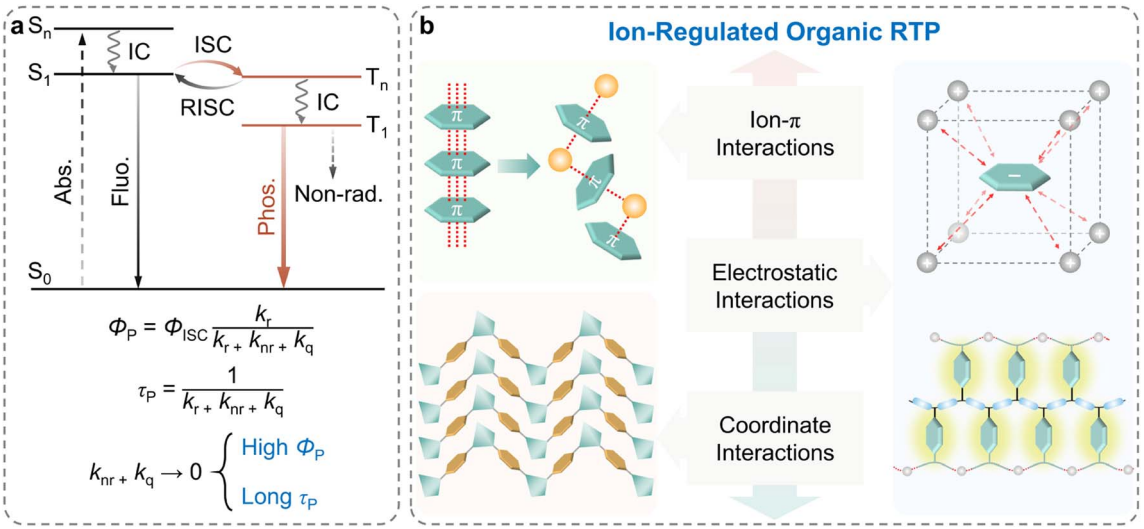

Scheme 1 (a) Simplified Jablonski diagram describing the photophysical processes of fluorescence and phosphorescence. (b) Classification of intermolecular interactions in ion-regulated organic RTP materials. Reproduced with permission from ref. 79 (copyright 2022, John Wiley and Sons), ref. 94 (copyright 2019, Springer Nature), and ref. 111 (copyright 2016, John Wiley and Sons).

ions and their phosphorescent properties, we summarize the recent progress in ion-regulated organic RTP materials from the perspective of weak intermolecular interactions (ion–π interactions), electrostatic interactions (in ionic crystals and ionic polymers), and coordinate interactions (Scheme 1b). The representative examples of ionic systems and their RTP properties are listed in Table 1. Please note that due to the introduction of valence and conduction bands in the inorganic parts altering the traditional RTP pathways, metal–organic compounds, such as metal–organic frameworks, metal–organic halides, and hybrid perovskites are not included in this perspective. These materials are, however, discussed in recent review articles which may be referred for detailed insights.[70–73] Finally, we illustrate the main issues and challenges for future developments in ionic RTP materials.

Ion–π interactions

Minimizing non-radiative transitions from the molecular motions is the key to obtaining long-lived phosphorescence (Scheme 1a, bottom).[1,74] Non-covalent intermolecular interactions, such as π–π interactions, n–π interactions, hydrogen bonds, *etc.*, are pivotal in organic neutral RTP systems, ensuring a rigid molecular environment that effectively impedes the non-radiative transitions of the excitons.[28,75–77] In comparison, ion–π interactions, a novel class of non-covalent bonding involving ions and aromatic groups, have attracted increased attention in the development of organic materials exhibiting high luminescence efficiency since their initial application in developing aggregation-induced emission systems in 2017.[78] Furthermore, the introduction of heavy halide anions (Cl^-, Br^-, and I^-) can further promote the SOC, thereby enhancing phosphorescence efficiency.[79]

In 2018, Tang *et al.* integrated the heavy-atom effect with anion–π interactions, proposing a novel approach for constructing purely organic RTP materials.[80] A series of highly luminescent organic salts were prepared by simply exchanging the counterions of TPO-P (Fig. 1a). In the solution state, all the compounds exhibited only short-lived fluorescence. However, in the crystalline state, the TPO-I and TPO-Br with heavy halide ions possessed long-lived phosphorescence with the lifetime of 48 μs and 706 μs and the quantum fields of 35.00% and 36.56%, respectively, while the compounds lacking the heavy halide ions only showed fluorescent properties (Fig. 1d and e). Single-crystal analysis and theoretical calculations revealed strong heavy-atom-participated anion–π interactions in the crystalline state for the TPO-I and TPO-Br (Fig. 1b and c). These interactions allowed the heavy atoms to approach the luminescent core closely, enhancing the SOC and charge transfer from the heavy halide ions to the π-conjugated TPO. This feature effectively increased the transition pathways between the singlet and triplet states, while reducing the energy gap between them, thereby boosting the ISC. Meanwhile, the short non-covalent interactions restricted the molecular motion, resulting in the efficient phosphorescence of the TPO-I and TPO-Br. Given the blue fluorescence-yellow phosphorescence dual-emission of the TPO-Br, a balance between the fluorescence and phosphorescence was achieved by incorporating the TPO-Br into various polymers to successfully result in high-performance white-light emission (Fig. 1f).

Introducing intramolecular/intermolecular charge transfer (CT) states is another effective approach to achieve high-efficiency phosphorescence.[81–83] According to Kasha's exciton model, the CT states can serve as intermediates for minimizing the energy gap between the lowest singlet and triplet states (ΔE_{ST}), thereby facilitating the ISC process.[1] Based on this strategy, in 2022, George *et al.* reported anion–π interaction-induced dual RTP emission in pyromellitic diimide (PmDI) derivative, BrPmDI.[84] The compound was synthesized through chemical modification of PmDI with bromine atom and iodide

Table 1 Typical examples of ion-regulated organic RTP systems and their phosphorescence properties[a]

Organic phosphors	Counterions	Wavelengths (nm)	Φ_P (%)	Lifetimes (ms)	References
1,2,3,4-Tetraphenyloxazolium (Fig. 1a)	I^- (TPO-I)	559	35.00	0.048	80
	Br^- (TPO-Br)	549	36.56	0.706	
Pyromellitic diimide (Fig. 1g)	I^- (BrPmDI in 5 wt% laponite)	470 (^{3}LE)	5.4	0.37	84
		560 (^{3}CT)		0.23	
Terephthalic acid (Fig. 2a)	NH_4^+ (AHT)	502	/	586	86
	Na^+ (DST)	508	/	585	
	K^+ (DPT)	456	/	504	
Tetraphenylphosphonium (Fig. 2e)	F^- (TPP F)	480	2	25.7	88
	Cl^- (TPP Cl)	500	2	108	
	Br^- (TPP Br)	486	4	6	
	I^- (TPP I)	430	42	0.0099	
	BF_4^- (TPP BF_4)	490	48	43.4	
	ClO_4^- (TPP ClO_4)	475	56	399.7	
Cytosine (Fig. 2f)	PO_4^- (Cy-PO_4)	430 (365), 495 (395)	/	126.1, 430.5	89
	Cl^- (Cy-Cl)	512 (365), 546 (395)	/	104.8, /	
Terephthalic acid (Fig. 3a)	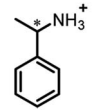 (TPA-(*R*/*S*)-PEA)	500	9.35	862	90
3,4-Methylenedioxyphenylamine (host)	Cl^-	477–679	1.40–18.7	71.3–1726	91
Ammonium salts (guest) (Fig. 3b)	Br^-				
Pyromellitic acid, mellitic acid (Scheme 2)	Na^+	447 (TSP)	66.9	168.3	74
	K^+	420 (TPP)	28.8	132.6	
	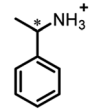	407 (HSM)	81.6	199.1	
		410 (HPM)	31.8	101.2	
		454 (TNP)	96.5	184.9	
Poly(styrene sulfonic acid)	Na^+, Li^+, K^+, Rb^+, NH_4^+, Mg^{2+}, Al^{3+}, Gd^{3+}, Ca^{2+}	540 (PSSNa)	0.79	894	94
Polyacrylic acid		480 (PAANa)	5.79	73 (τ_1), 222 (τ_2) 596 (τ_3), 2139 (τ_4)	
Polymaleic acid		523 (PMANa)	2.77	378	
Poly(maleic acid-*co*-4-styrenesulfonic acid) (Fig. 4a and d)		500 (PMANa-*co*-PSSNa)	13.08	385	
Poly(4-vinylpyridine) (Fig. 4e)	SO_3^- (PVP–S)	524–572	6.40	80.32–578.3	95
Poly(phenylpropenes-*co*-maleic anhydride) (Fig. 5a)	Na^+ (*h*-PMM-Na)	498	/	401	96
	K^+ (*h*-PMM-K)	500	/	345	
Cellulose (Fig. 5b)	Mg^{2+}	530	5	50	102
Cellulose 1-cyanomethylimidazolium chloride (Fig. 5c)	Cl^-	550	11.81	158	103
Hemicellulose, lignin, cellulose (Fig. 5d)	Cl^-	545	4.7	17.5–297	105

Table 1 (*Contd.*)

Organic phosphors	Counterions	Wavelengths (nm)	Φ_P (%)	Lifetimes (ms)	References
Chitosan (Fig. 6)	Na^+, K^+, Mg^{2+}, Ca^{2+}, Zn^+, Y^{3+}	500	0.12–1.5	159–1041	106
Poly-diallyldimethylammonium (host)	Cl^-	555 (NpA@PAB)	4.40	3.72	107
Commercial fluorescent dyes (guest) (Fig. 7a)	Br^-	528 (S-BN@PAB)	17.2	25.9	
		538 (HCM@PAB)	31.6	10.7	
		510 (QN@PAB)	13.6	13.0	
		700 (RhB@PAB)	27.1	6.10	
		581 (PF@PAB)	1.8	4.95	
Sodium alginate (host)	Na^+	430–540	3.2–25.7	310–1200	108
Aromatic sodium carboxylates (guest) (Fig. 7c)					
Terephthalic acid	Zn^{2+}	484–533	2.2–3.4	75–1321	112
Isophthalic acid	Cd^{2+}				
Trimesic acid (Fig. 8a and b)					
Chiral L-histidine (Fig. 8g)	Zn^{2+}	465–678	9.54–21.59	141.9–356.7	114
4,5-Dicyanoimidazole (Fig. 9a)	Zn^{2+} (Zn-DCI)	536	75	197.15	115
	Cd^{2+} (Cd-DCI)	441	58.4	630.15	
Crown ether (Fig. 10a)	K^+	490 (B15C5⊃K^+)	/	420	119
		490 (DB18C6⊃K^+)	/	330	
		470 (DB24C8⊃K^+)	/	210	
		470 (DB30C10⊃K^+)	/	950	
Phenoxathiine (host)	Zn^{2+}	580	7.40–20.4	56.9–349	120
Polyphenylquionline (guest) (Fig. 10d)					
Benzophenone (host)	Al^{3+}, $Cu^{+/2+}$, Zn^{2+}, Ga^{3+}, Ag^+, Cd^{2+}, In^{3+}	512–574	1.4–70	27–313	121
Phenylquinoline (guest) (Fig. 10e)					

[a] Note: '/' refers to the relevant information was not provided in the references.

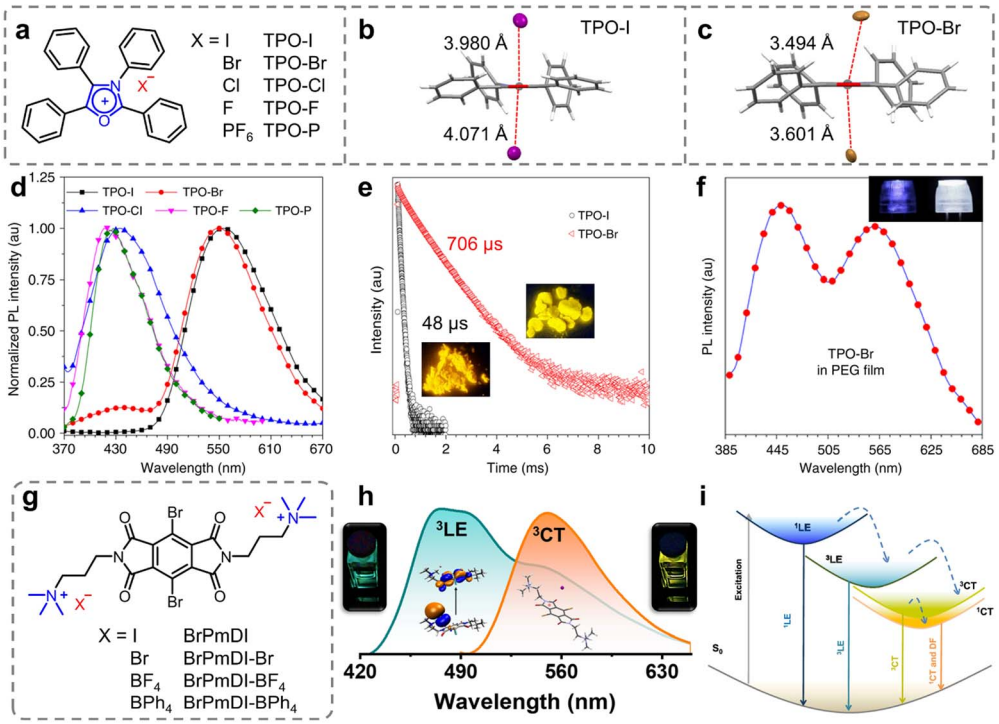

Fig. 1 (a) Chemical structures of TPO-I, TPO-Br, TPO-Cl, TPO-F, and TPO-P. Anion–π interactions with distances for (b) TPO-I and (c) TPO-Br. (d) PL spectra of TPO-I, TPO-Br, TPO-Cl, TPO-F, and TPO-P in the solid state. (e) Time-resolved PL decay of d TPO-I and TPO-Br (insets: photographs of TPO-I and TPO-Br were taken under 365 nm UV irradiation). (f) PL spectra of the PEG film containing TPO-Br (2%, m/m) (insets: photographs of 3D printed lampshades without (left) and with (right) TPO-Br taken under UV-LED lamps). (g) Chemical structures of BrPmDI with different counterions. (h) Normalized PL emission spectra at different excitation wavelengths of 370 nm (cyan line) and 470 nm (orange line) showing the contribution both LE and CT emissions. (i) Jablonski diagram showing various emission processes possible from the LE state of the PmDI core and anion–π-induced CT states. Reproduced with permission from (a–f) ref. 80 (copyright 2018, Springer Nature) and (g–i) ref. 84 (copyright 2022, American Chemical Society).

counterions (Fig. 1g). Notably, in the BrPmDI single crystals, I^- was found stabilized by anion–π interactions of 3.69 Å length within the cationic π-conjugated layers. Meanwhile, the photophysical experiments and theoretical calculations further confirmed the formation of anion–π interaction-induced emissive CT states. Consequently, the researchers effectively embedded the BrPmDI molecules into the supramolecular scaffolding (LAPONITE®) effectively to stabilize the triplet excited states, ultimately achieving dual solution-phase phosphorescence emission from the locally excited (^{3}LE, 470 nm) and the anion–π interaction-induced CT (^{3}CT, 560 nm) triplet states (Fig. 1h and i). This study further demonstrated the feasibility of utilizing ion–π interactions in developing various highly efficient RTP materials and modulating their properties.

Electrostatic interactions

Compared to ordinary neutral systems, organic ionic crystals and polymers are constructed by ionic bonding and ionic cross-linking, which are a kind of electrostatic interaction between an anion and a cation.[28] These strong interactions not only construct a rigid environment to restrict molecular motion, but also prevent the quenching effects caused by oxygen and moisture, effectively suppressing the non-radiative relaxation of the triplet excitons. Moreover, the electronic structures of ionic systems are more easily manipulated through charge-state adjustments, allowing for flexible molecular design and optimized RTP performance.

Organic ionic crystals

In ionic crystals, in addition to ion–π interactions, there is a widespread presence of strong electrostatic interactions known as ionic bonding. Compared with hydrogen bonding, this type of interaction exhibits distinct properties such as stronger bonds, lack of directional constraints, and non-saturation. The strength of the ionic bonds surpasses that of hydrogen bonds, providing a more rigid environment.[85] Such rigidity is crucial in minimizing the non-radiative decay of the triplet excitons. In 2018, Huang *et al.* introduced a new class of organic ionic crystals, which exhibited intense and ultralong RTP under ambient conditions (Fig. 2a).[86] The unique ionic bonding in the organic salts promoted an ordered arrangement to enhance molecular aggregation crucial for the RTP emissions. More importantly, the study demonstrated that changing the cations from NH_4^+ to Na^+, and K^+ allowed for tunable phosphorescence colors from yellow-green to sky blue, with emission lifetimes over 586 ms (Fig. 2b–d). Additionally, the research demonstrated the potential for reversible RTP through alternate exposure to ammonia and hydrogen chloride gases,

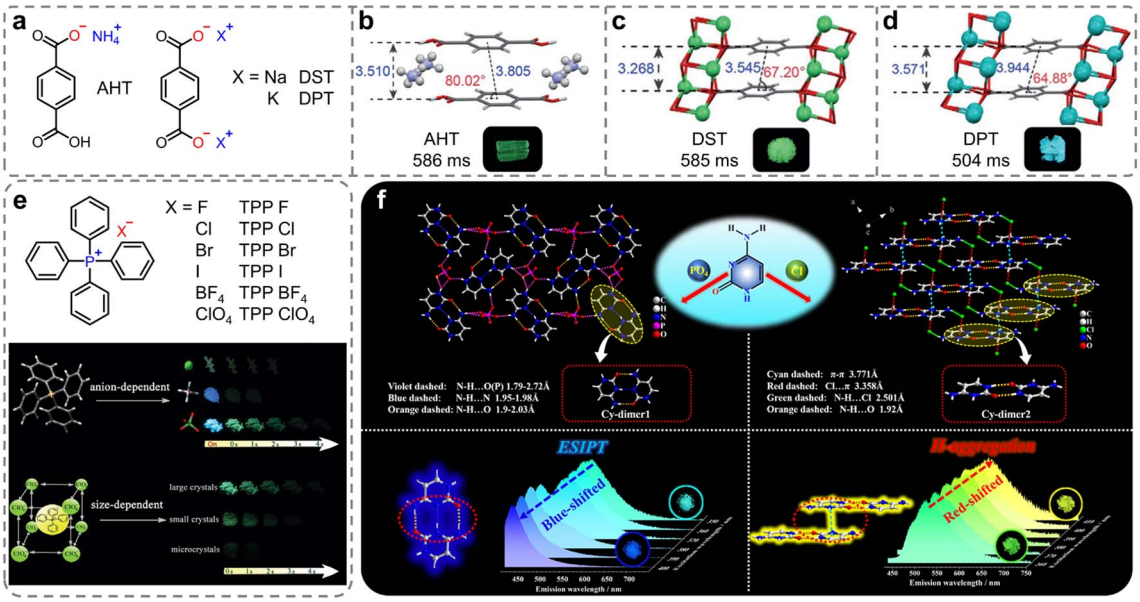

Fig. 2 (a) Chemical structures of ionic compounds AHT, DST, and DPT. Molecular packing of (b) AHT, (c) DST and (d) DPT in dimer and the photographs of the ionic crystals under 365 nm lamp off. (e) Chemical structures of ionic compounds TPP X (insets: the schematic illustration of anion-regulated and size-dependent afterglow of tetraphenylphosphonium perchlorate crystals). (f) Schematic representation and single-crystal structures for constructing color-tunable ionic cytosine complexes. Reproduced with permission from (a–d) ref. 86 (copyright 2018, John Wiley and Sons), (e) ref. 88 (copyright 2019, Royal Society of Chemistry), and (f) ref. 89 (copyright 2022, American Chemical Society).

suggesting applications in visual gas sensing. This strategy allowed for the tuning of phosphorescence color and lifetime by altering the counterions, which contributed to expand the range of ultralong RTP materials as well as their applications. Using the same strategy, Qian *et al.* also reported persistent phosphorescence regulated by anions with tetraphenylphosphonium (TPP^+) cations (Fig. 2e).[87,88] The strong ionic bonding interactions between the TPP^+ and anions were instrumental in facilitating the afterglow generation. Moreover, TPP ClO_4 also exhibited size-dependent ultralong afterglow (Fig. 2e).

In 2022, Yan *et al.* introduced a novel category of two-component ionic crystals created through self-assembly of cytosine (Cy) with phosphate (PO_4^-) and halogens anions (Cl^-), named Cy-PO_4 and Cy-Cl, respectively.[89] The intermolecular interactions of cytosine with the anions led to diverse energy levels and crystal stacking modes, which controlled the molecular aggregation (H-aggregation) and the excited-state intermolecular proton transfer (ESIPT) process. In the Cy-PO_4 crystal, cytosine molecules formed a coplanar dimer configuration (Cy-dimer1, Fig. 2f, left) that enabled the ESIPT crucial for the keto–enol transition. For Cy-Cl, face-to-face H-aggregated dimers (Cy-dimer2, Fig. 2f, right), reinforced by π–π interactions, were pivotal for the stabilization of the triplet excitons. Consequently, the H-aggregation-induced green to yellow RTP for Cy-Cl and ESIPT-dominated cyan RTP to deep blue thermally activated delayed fluorescence in Cy-PO_4 can be achieved through control of the excitation wavelength, time evolution, and temperature. This work developed a new strategy for color-tunable afterglow from static and dynamic perspectives and has potential applications in information storage and anti-counterfeiting technology.

Besides inorganic ammonium cations, organic ammonium cations have been also applied as counterions in constructing efficient RTP materials. In 2018, Duan *et al.* reported chiral organic ionic crystals derived from terephthalic acid (TPA) and chiral α-phenylethylamines (PEA) exhibiting persistent circularly polarized phosphorescence.[90] At room temperature, these ionic crystals exhibited distinct green phosphorescence with lifetimes of up to 862 ms (Fig. 3a). It is noteworthy that the TPA-(*R*/*S*)-PEA crystals exhibited significant circularly polarized luminescence signals in both the fluorescence and phosphorescence regions, with the asymmetry factor reaching $\approx 10^{-2}$. Single-crystal analysis revealed that the strong intermolecular interactions between terephthalic acid and chiral amines produced asymmetric torsion angles, which favored the generation of chiral triplet excitons and, thus, exhibited distinct persistent circularly polarized phosphorescence properties. Following that, Lin *et al.* developed novel metal-free, two-dimensional layered organic ammonium halide crystals (Fig. 3b, HLB and HLC).[91] The rigid laminates were composed *via* various ionic bonding interactions between the ammonium and halide ions. These interactions significantly restricted the molecular motion, which endowed it with significant green RTP. By introducing ammonium halides with diverse triplet energies as guests into phenylethylamine salt hosts, full-color including white persistent phosphorescence emission with Φ_P and lifetime up to 18.7% and 1.7 s was achieved, respectively. This phenomenon can be attributed to an efficient Förster energy transfer between the host and guest, and yielding highly efficient RTP of guests (Fig. 3c). Meanwhile, the energy transfer efficiency between the guest and the host in the doped materials strongly depends on the overlapping range of the absorption

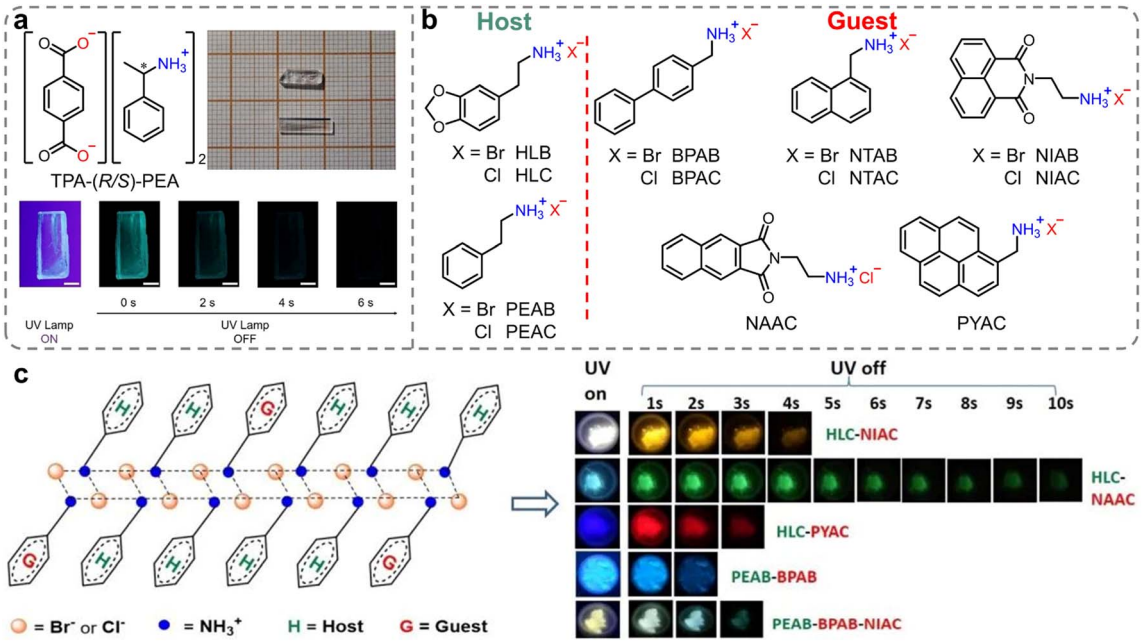

Fig. 3 (a) Chemical structures of TPA-(*R*/*S*)-PEA organic ionic crystals (insets: images of TPA-(*R*/*S*)-PEA crystals in bright field, under UV irradiation and after excitation for different times). (b) Molecular structure of host and guest ammonium halides. (c) Structure diagram of the host–guest system and afterglow photos of doped halides under a UV lamp. Reproduced with permission from (a) ref. 90 (copyright 2018, John Wiley and Sons) and (b and c) ref. 91 (copyright 2021, Royal Society of Chemistry).

band of the guest and the emission band of the host. Finally, the authors applied it to various complex anti-counterfeiting and dual-mode fluorescent/phosphorescent chemical sensors.

It is noteworthy that the H-aggregation strategy in previous works mainly focused on enhancing the RTP performance by strengthening the π–π interactions within the crystal.[34,92,93] While the strong π–π interactions between the adjacent phosphorescent chromophores can effectively stabilize the triplet excitons, the substantial dissipation of excitons through the triplet–triplet annihilation channel results in a lower RTP efficiency and a bathochromic shift of phosphorescence.[35] This effect seriously impedes to develop deep-blue organic RTP emitters. An *et al.* presented a strategy for achieving high-efficiency blue phosphorescence by confining isolated chromophores in ionic crystals.[74] Pyromellitic acid and mellitic acid with rich carboxyl groups were ionized by sodium hydroxide, potassium hydroxide and alpha-methylbenzylamine to form ionic crystals (Scheme 2). Taking tetrasodium pyromellitate (TSP) crystal as an example, it exhibited intense blue phosphorescence at 450 nm with a quantum efficiency of 66.9%. Single-crystal analysis revealed that the chromophores were isolated by the surrounding Na^+ through multiple ionic bonds, forming a cage-like structure. This architecture not only suppressed the molecular motion of the chromophores but also segregated the chromophores with negligible inter-chromophore interactions, thereby achieving high phosphorescence efficiency. Remarkably, tunable phosphorescence colors from blue to deep blue with Φ_P up to 96.5% were achieved by altering the charged chromophores and their counterions.

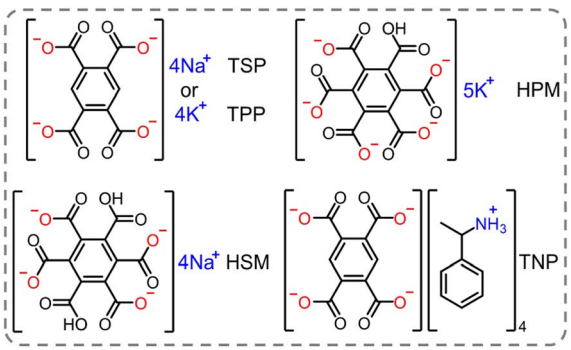

Scheme 2 Chemical structure of the ionic crystals (TSP, TPP, HSM, HPM and TNP).

Ionic polymers

Apart from organic ionic crystals, the strong ionic bonding and ionic cross-linking interactions present in ionic polymers can restrict the molecular motion, thus decreasing the non-radiative decay of the triplet excitons. In 2019, Huang *et al.* proposed a simple strategy to achieve ultralong phosphorescence in polymers *via* ionic cross-linking (Scheme 1b).[94] They initially constructed sodium polystyrene sulfonate (PSSNa) as an ionic model polymer. As shown in Fig. 4a, under ultraviolet (UV) light of 365 nm wavelength, PSSNa film exhibited sky-blue fluorescence and yellow afterglow, closely related to the ionic cross-linking of the sulfonate sodium substituents. Impressively, multicolor long-lived phosphorescent emissions were achieved by tuning the excitation wavelength, with the afterglow colors adjustable from blue to orange at 77 K, originating from

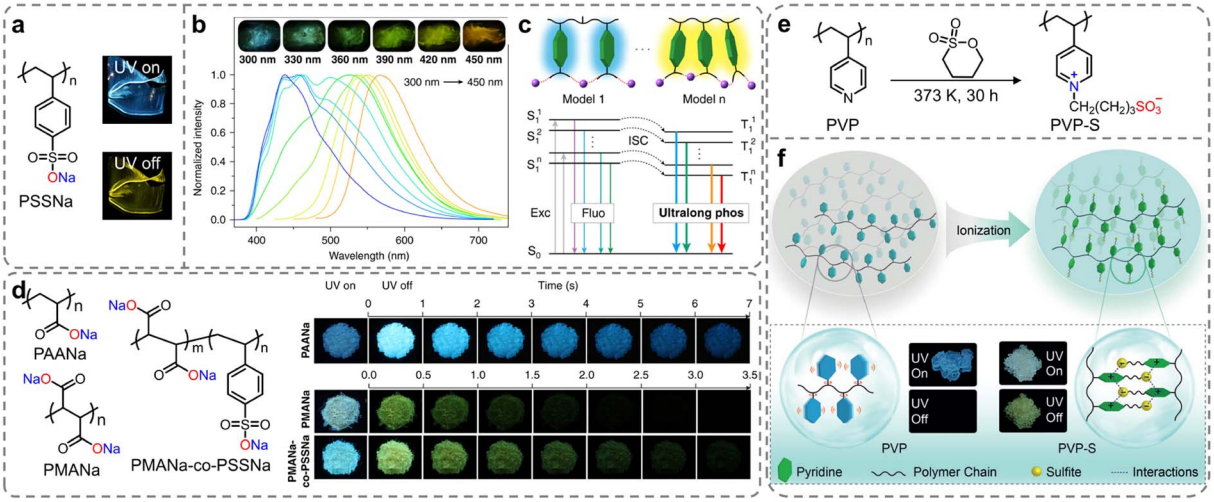

Fig. 4 (a) Molecular structure of PSSNa polymer (insets: photographs of PSSNa solids taken under a 365 nm lamp on and off). (b) Excitation dependent phosphorescence spectra of PSSNa polymer at 77 K (insets show photographs taken after PSSNa polymer excited by 300, 330, 360, 390, 420, and 450 nm at 77 K). (c) Proposed mechanism for multicolor ultralong phosphorescence as the excitation wavelength changed. (d) Molecular structures of PAANa, PMANa, and PMANa-*co*-PSSNa (insets: photographs of PAANa, PMANa, and PMANa-*co*-PSSNa polymers taken before and after the irradiation of a 310 nm UV lamp). (e) Synthesis of the PVP-S polymer. (f) Ionization enabling ultralong organic phosphorescence in polymers. Reproduced with permission from (a–d) ref. 94 (copyright 2019, Springer Nature) and (e and f) ref. 95 (copyright 2019, John Wiley and Sons).

different phosphorescent centers (Fig. 4b). Experimental data and theoretical calculations showed that introducing ionic bonding interactions in polymers effectively inhibited the molecular motion of the aromatic luminescent groups, ensuring efficient emission from various phosphorescent centers (Fig. 4c). Moreover, phosphorescence signals of the PSSNa polymer could still be detected even at a temperature of 443 K, owing to strong ionic bonding interactions. This design concept could be applied to both aromatic and non-aromatic polymer systems, namely PAANa, PMANa, and PMANa-*co*-PSSNa. With the chromophore variations, the RTP emission colors were successfully tuned from yellow to blue (Fig. 4d). Under ambient conditions, the lifetimes of blue RTP emission band at 480 nm for PAANa were reaching up to 2139 ms (τ_4, Table 1). The research enhanced the properties of traditional polymer materials and had great application prospects in fields like flexible displays, lighting, data encryption, and biomedicine, due to the wide availability and low cost of polymeric materials. Following this study, to further demonstrate the universality of color-adjustable phosphorescence *via* ionic bonding cross-linking strategy, they investigated the effects of sulfonation on the photophysical properties of another amorphous polymer poly(4-vinylpyridine) (PVP) (Fig. 4e).[95] After ionization with 1,4-butanesultone, the PVP-S phosphor exhibited an ultralong organic phosphorescence lifetime of 578.36 ms, which was 525 times longer than that of the unmodified PVP (Fig. 4f). Additionally, excitation-dependent color-tunable phosphorescence was also observed at both room temperature and 77 K, with emission colors ranging from blue to red. The facile and feasible chemical ionization strategy opened up new avenues for the development of organic smart RTP polymers.

Similar to the aforementioned strategy, Deng *et al.* achieved ultralong RTP emission in bio-based non-conjugated polymers through a simple hydrolysis process (Fig. 5a).[96] The bio-based polymer was synthesized *via* free radical solution copolymerization using biomass phenylpropenes and maleic anhydride as monomers. This as-prepared polymer with no traditional luminescent groups could emit blue fluorescence. It is noteworthy that the polymer, after undergoing hydrolysis in a sodium hydroxide solution, exhibited significant enhancement in its fluorescence and afterglow, with a lifetime of 401 ms (Fig. 5a). Furthermore, the type of metal cations in the carboxylate notably affected the phosphorescent properties of the hydrolyzed product.

Unlike the traditional organic conjugated luminescent molecules with extended π-structures, non-traditional luminescent molecules are non-conjugated compounds with electron-rich subunits and have drawn increasing attention in recent years.[97] Owing to the enhancement of SOC by heteroatoms, these non-traditional luminescent molecules, characterized by clustering-triggered emission characteristics, are potential materials for realizing RTP.[98–100] Among these, cellulose, a naturally occurring renewable resource known for its low toxicity and environmental friendliness, has gained widespread interest.[101] However, due to the lack of conjugated groups, the cellulose exhibits weak absorption and low luminescence quantum yields. In 2022, Tian *et al.* proposed an effective method to enhance the phosphorescence of cellulose (Fig. 5b).[102] By doping halide salts into cellulose, the absorption transition from halide anions to polysaccharide chains was induced, along with an increase in the ISC *via* the external heavy-atom effect. Moreover, the inclusion of divalent metal ions within cellulose effectively minimized the non-radiative

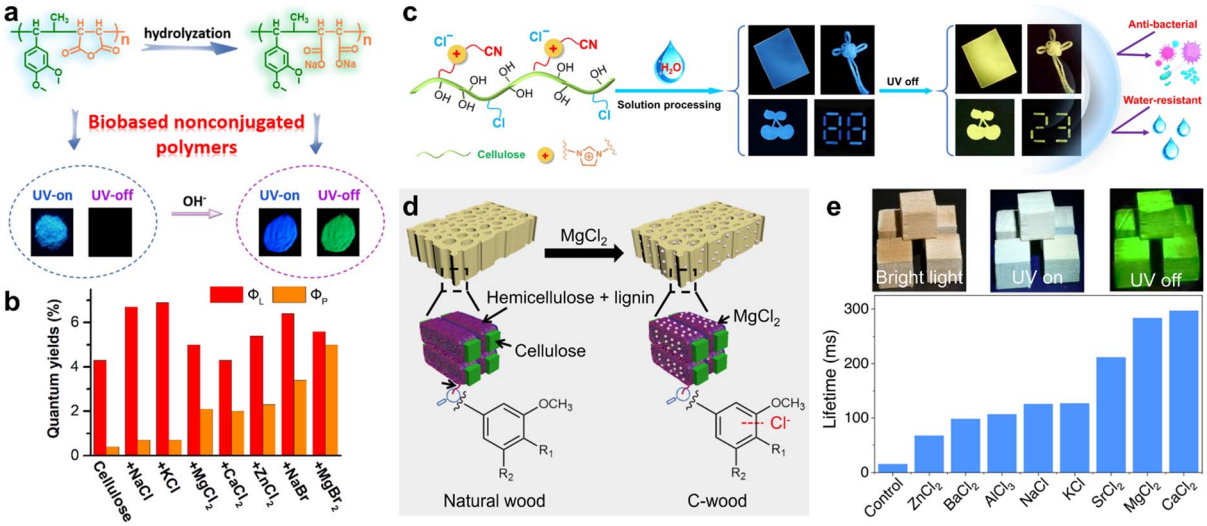

Fig. 5 (a) Schematic illustration and the photographs for preparing biomass copolymers. (b) Total luminescence and phosphorescence quantum yields of dried cellulose doped with salts. (c) Chemical structure, processability, and performance of the cationic cellulose derivative with RTP property. (d) Schematic showing the preparation of room temperature phosphorescent C-wood from natural basswood. (e) Photographs of C-wood under bright field (left), UV irradiation (middle), and after switching off the UV light (right), and the lifetime of C-wood prepared using different salts. Reproduced with permission from (a) ref. 96 (copyright 2021, American Chemical Society), (b) ref. 102 (copyright 2022, American Chemical Society), (c) ref. 103 (copyright 2022, Springer Nature), and (d and e) ref. 105 (copyright 2023, Springer Nature).

relaxations *via* electrostatic interactions. Consequently, the Φ_P of $MgBr_2$-doped dry cellulose could reach up to 5% (Fig. 5b). Zhang *et al.* developed a cationic phosphorescent cellulose derivative by introducing ionic moieties, such as cyanomethylimidazolium cations and chloride ions into the cellulose chains (Fig. 5c).[103] The cyano group and nitrogen atoms in the imidazolium cations facilitated the ISC process. Furthermore, the multiple interactions between the cyano groups, chloride ions, and cellulose's hydroxyl groups, through hydrogen bonding and electrostatic forces, effectively suppressed the non-radiative transitions, leading to excellent RTP performance with a maximum Φ_P and lifetime of 11.81% and 158 ms, respectively. Additionally, adding a small amount of glutaraldehyde to the cationic cellulose solution could form a stable dual cross-linked structure, resulting in phosphorescent patterns with superior antimicrobial and water-resistant properties (Fig. 5c). More recently, they also successfully constructed tunable excitation-dependent and visible-light-excited ultralong RTP materials by manipulating the aggregated state of anionic cellulose trimellitates.[104]

Chen *et al.* demonstrated a sustainable method to create RTP materials from natural wood using external chloride anion treatment (Fig. 5d).[105] Specifically, treating wood with $MgCl_2$ aqueous solution at room temperature resulted in wood containing chloride ions (named C-wood, Fig. 5d), where the halide chloride ions could enhance the SOC and increased the phosphorescence lifetime. The C-wood consequently exhibited intense RTP emission with a lifetime of 297 ms, which was nearly 17 times longer than that of the natural wood (Fig. 5e). Similarly treated with various other chloride anion salts, the treated woods exhibited prolonged phosphorescence lifetimes in comparison to the untreated form (Fig. 5e).

In non-aromatic resources, aside from cellulose, chitosan is a highly biocompatible polymer composed of aminoglucose monomers that was extensively utilized as a hydrophilic matrix due to its easily accessible (Fig. 6a).[101] The chemical structure of chitosan facilitates easy physical or chemical modifications. Moreover, the incorporation of functional groups such as amino, hydroxyl, and carbonyl within the chitosan structure promotes the generation of oxygen clusters, which are advantageous for RTP emission. In 2016, Zhang *et al.* demonstrated

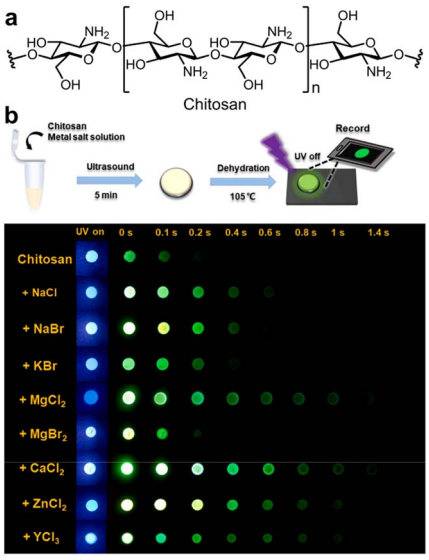

Fig. 6 (a) Structure of chitosan. (b) Luminescence imaging of dried chitosan doped with different metal halide under a UV lamp (365 nm) on and off. Reproduced with permission from ref. 106 (copyright 2023, Elsevier).

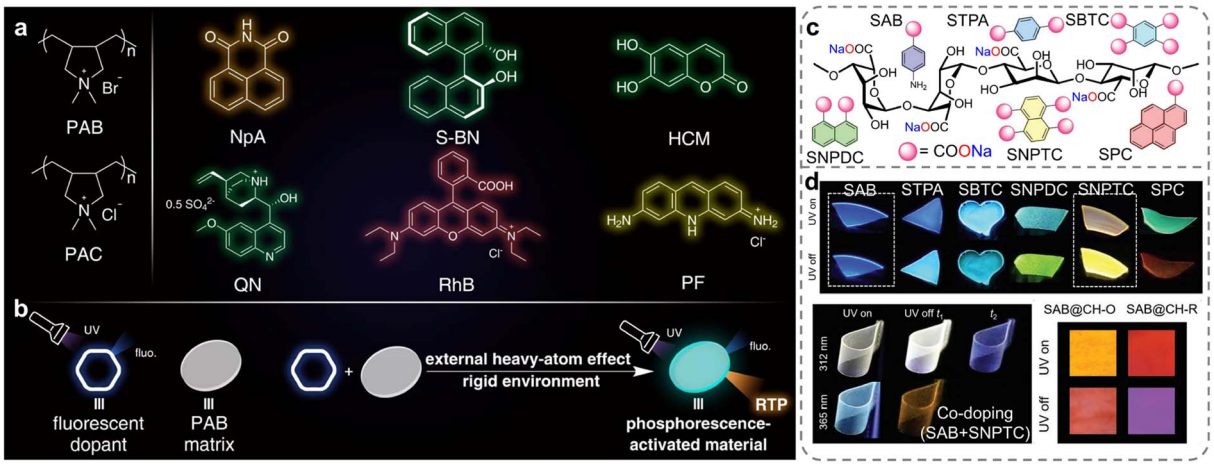

Fig. 7 (a) Structures of the polymers (PAB and PAC) and the dopants: NpA, S-BN, HCM, QN, RhB and PF. (b) Illustration of the general strategy. (c) Structures of the aromatic sodium carboxylates and SA. (d) Luminescence photographs of single-component-doped, co-doped, and TS-FRET SA films with multicolor and multi-tunable afterglows. Reproduced with permission from (a and b) ref. 107 (copyright 2021, John Wiley and Sons) and (c and d) ref. 108 (copyright 2022, John Wiley and Sons).

that N-substituted naphthalimides conjugated with chitosan exhibited RTP properties and found practical application in time-resolved bioimaging.[81] In 2023, Tian *et al.* also investigated the enhancement and control of chitosan's RTP properties by physically mixing halide salts (Fig. 6b).[106] Notably, the RTP characteristics of the chitosan could be precisely adjusted by altering the concentrations and types of halide salts. The presence of cations in the halide salts enhanced RTP by binding with hydroxyl groups, minimizing the distance between halide ions and the emissive clusters, thus boosting the external heavy-atom effect. Moreover, this interaction could also increase the rigidity of the matrix, favorably influencing RTP emissions.

Compared to chemical modification, direct doping of chromophores into ionic polymers is considered a more straightforward and quantifiable method for preparing RTP materials and modulating their properties.[27] The presence of a robust ionic bonding network in polymers is considered highly effective for stabilizing excited triplet excitons, thereby facilitating the generation of RTP emission. Ma *et al.* constructed a series of organic doped RTP systems by incorporating commercial fluorescent dyes into ionic polymer matrix with external heavy-atom effects and rigid ionic bonding network (Fig. 7a and b).[107] This poly-diallyldimethylammonium bromide (PAB) matrix containing bromide ions facilitated the ISC process *via* an external heavy-atom effect in the doped systems, leading to the generation of excited triplet states. Concurrently, a rigid ionic bonding network formed between the bromide anions and the quaternary ammonium cations in the polymer played a crucial role in reducing the non-radiative deactivation, contributing to the generation of effective RTP emissions. This work offered a practical approach for developing purely organic RTP polymers without the use of complex processes. Based on the same strategy, Yuan *et al.* developed amorphous sodium alginate (SA) doped with various aromatic sodium carboxylates, which allowed for easy and fast fabrication of flexible, transparent, redissolvable polymer films with multi-tunable afterglow colors, ranging from blue to red and even white (Fig. 7c).[108] The formation of strong hydrogen and ionic bonds between the SA chains and the doped phosphors impeded the molecular motion. Furthermore, the excitation- and time-dependent afterglows could be achieved and controlled by adjusting the doping concentration, co-doping, and utilizing the triplet to singlet Förster resonance energy transfer (Fig. 7d). This innovative approach demonstrated potential in advanced multimode anti-counterfeiting applications, offering a significant advancement in the field of smart luminescent materials.

Coordinate interactions

Coordinate bonding, a unique type of covalent bond, where only one atom provides the electron pairs for bonding, is prevalent in organometallic compounds.[109] Strong coordinate bonding interactions create rigid architectures for the chromophores, which are crucial for reducing the non-radiative decay of triplet excitons.[110] Meanwhile, the coordinate inorganic metals can facilitate the SOC due to the heavy-atom effect, thereby extending the phosphorescence lifetime and enhancing the phosphorescence efficiency.[111] Moreover, manipulation of the metal centers and ligands allows tuning of the photophysical properties, including the emission wavelength and lifetime.

Coordination polymers, differ from purely organic materials, being formed through coordinate bonding between organic ligands and metal coordination ions. Due to their tunable and stable characteristics, coordination polymers have been used in various applications like sensors, displays, and bioimaging.[70] In 2016, Yan *et al.* demonstrated a significant enhancement in long-lived RTP properties of aromatic acids through coordinate bonding interactions with common metal ion, like Zn^{2+}.[112,113] The coordinate bonding formed between Zn^{2+} and terephthalic acid (TPA) played a crucial role in reducing the non-radiative deactivation. As shown in Fig. 8a, the TPA molecules were tightly encapsulated within the Zn-based rigid framework, effectively

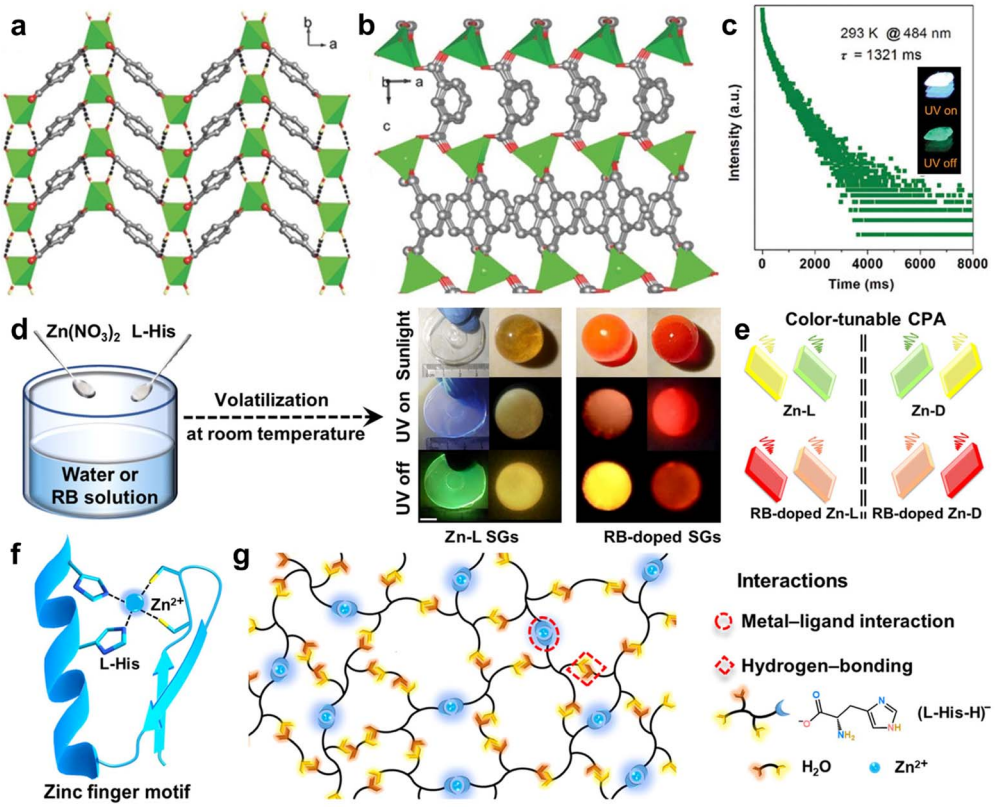

Fig. 8 Crystal structures of (a) Zn-TPA and (b) Zn-IPA. (c) Time-resolved emission decay curve (484 nm) for Zn-IPA under ambient conditions. (d) Preparation of Zn-L and RB-doped SGs, and photos of the obtained Zn-L and RB-doped SGs taken under the sunlight, and before and after UV-light turned off. (e) Multicolored CPA emissions from chiral SGs. Spiral lines represent circularly polarized afterglow-active signals. (f) C_2H_2-type zinc finger motif. (g) Schematic representation of the SGs assembly. Reproduced with permission from (a–c) ref. 112 (copyright 2016, John Wiley and Sons) and (d–g) ref. 114 (copyright 2023, Springer Nature).

inhibiting the non-radiative transitions and boosting the RTP emission.[112] Moreover, the organic–metal coordination polymers displayed tunable phosphorescence by varying the metal ions and aromatic ligands, achieving an RTP lifetime of up to 1.3 s (Fig. 8b and c). This work offered a cost-effective way to produce high-performance RTP metal–organic hybrid materials without relying on noble or rare-earth metals, which can be favorable to illumination and sensor applications. Recently, they designed and prepared a series of supramolecular glasses (SGs) based on zinc-L-histidine complexes using an evaporation-induced self-assembly strategy (Fig. 8d).[114] The formation of SGs was primarily driven by the synergistic effect of strong coordinate bond and hydrogen bond among Zn^{2+}, L-histidine, and H_2O (Fig. 8g). These interactions endowed the SGs with color-tunable circularly polarized afterglow ranging from blue to red with an asymmetry factor as high as 9.5×10^{-3} and a lifetime of up to 356.7 ms (Fig. 8e and f). This work not only presented the SGs with broad tunability in the afterglow and significant circular polarization but also introduced an evaporation-induced self-assembly approach for the macroscopic self-assembly of chiral organic–metal hybrids for photonic applications.

In addition to typical aromatic acids, other organic compounds are also viable as organic ligands for constructing coordination polymers with RTP performance. In 2022, Yan

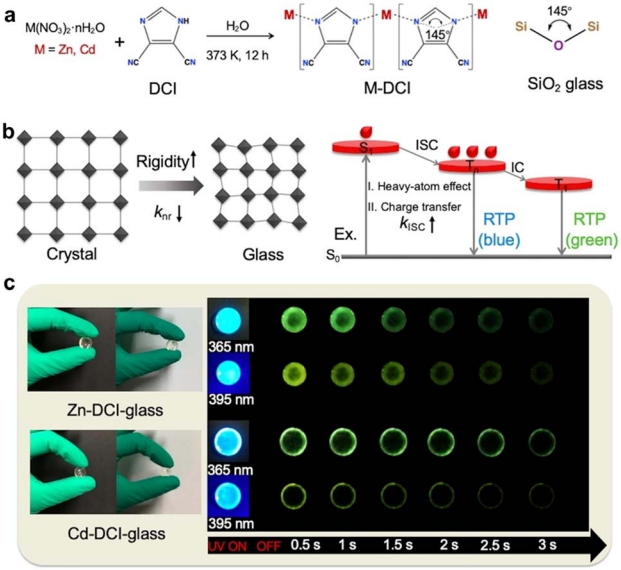

Fig. 9 (a) The synthetic procedure of glasses compared to the basic Si–O–Si building unit in classical inorganic zeolites. (b) Schematic mechanism of highly efficient RTP of glasses highlighting the rigid molecular environment for inhibiting non-radiative relaxation and the enhanced ISC process for harvesting triplet excitons. (c) Photographs of the glasses taken before and after turning off the UV light (365 nm and 395 nm). Reproduced with permission from ref. 115 (copyright 2022, John Wiley and Sons).

et al. developed transparent bulk glasses with an extended phosphorescence lifetime of 630.15 ms and a high photoluminescence quantum yield of up to 75% at ambient conditions *via* the bottom-up supramolecular coordination self-assembly strategy (Fig. 9a).[115] These glasses, comprising metal ions (Zn^{2+} and Cd^{2+}) and imidazolate-based ligands, featured a structure resembling the random network SiO_2 glasses (Fig. 9a). The study revealed that these hybrid glass materials possessed a high Young's moduli and hardness, providing a rigid network that reduced the non-radiative transitions of triplet excitons, thereby enhancing the phosphorescence efficiency (Fig. 9b). Moreover, the luminescence of these hybrid glasses was not a mix of fluorescence and phosphorescence but a full phosphorescent emission directly originating from various triplet state energy levels, demonstrating a high utilization rate of triplet excitons in the materials (Fig. 9c).

Dynamic coordinate bonds are a type of bonding used in coordination chemistry.[109] These form between metal ions and organic ligands, but unlike traditional coordination bonds, dynamic coordination bonds can form and break rapidly and reversibly. This dynamic nature is crucial in the processes of self-assembly, self-healing, responsive polymers, and the design of smart materials.[116–118] In 2019, Tang *et al.* discovered that a series of crown ethers with different ethylene glycol chains exhibited RTP in the crystalline state (Fig. 10a).[119] The flexible glycol chains of crown ethers imparted characteristic ionic selectivity, which combined with the crystallization tendency, allowed for morphological control of the crystalline state, enabling tunable phosphorescence. When K^+ was integrated into crown ethers, the phosphorescence lifetime could increase. The mechanism of K^+ response was related to the strong coordinate interaction between the multiple oxygen atoms in the crown ether and K^+, suppressing non-radiative relaxation (Fig. 10b). Additionally, the phosphorescence lifetime of crown ethers complexed with K^+ increased with the length of the glycol chain. Utilizing this "activated" phosphorescence, the authors constructed an advanced multi-level information encryption system in the solid state, where the inherent guest responsiveness of crown ethers allowed for precise design and fabrication of more intelligent luminescent materials (Fig. 10c).

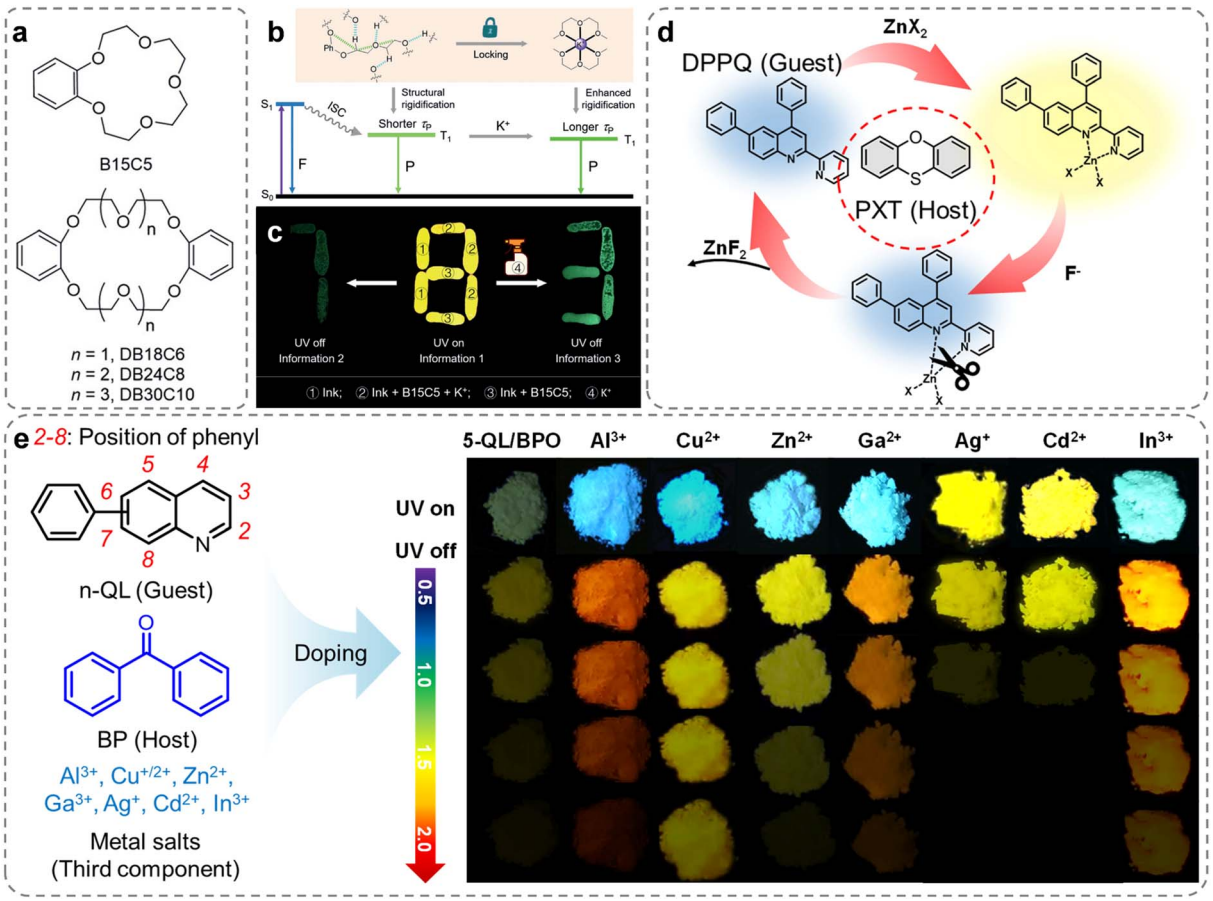

Fig. 10 (a) The molecular structures of crown ethers with different ethylene glycol chains. (b) Theoretical models based on Jablonski diagram for understanding the performance of crown ether-based tunable RTP in the solid state. (c) Photograph shows advanced-encryption application based on K^+ "activated" persistent phosphorescence strategy. (d) Schematic diagram and molecular structures of host and guest molecule for dynamic manipulation of RTP properties. (e) Molecular structures of the different components and the photographs of three-component doped materials composed of 5-QL/BP and various metal salts under 365 nm UV light on and off. Reproduced with permission from (a–c) ref. 119 (copyright 2019, John Wiley and Sons), (d) ref. 120 (copyright 2023, John Wiley and Sons), and (e) ref. 121 (copyright 2022, American Chemical Society).

In 2022, Dong *et al.* introduced an effective approach by incorporating dynamic metal–ligand coordination into host–guest doped systems, offering a means to fabricate regulated RTP materials with controlled properties (Fig. 10d).[120] The addition of a minimal amount of Zn^{2+} in the three-component doped system demonstrated remarkable phosphorescence performance. Through single-crystal analysis and theoretical calculations, it was revealed that the coordinate interactions significantly augmented the SOC of the guest, leading to an elevated ISC rate and phosphorescent radiative rate. By manipulating the Zn^{2+} counterions and adjusting the doping ratio of the guest, facile modulation of luminous color and Φ_P could be achieved. Additionally, the reversible nature of metal–ligand coordinate interactions enabled dynamic manipulation of coordination-activated and dissociation-deactivated RTP (Fig. 10d). Employing a similar approach, a series of three-component doped systems were assembled by introducing phenylquinoline isomers (n-QL) as the guest molecules and seven metal ions (Al^{3+}, $Cu^{+/2+}$, Zn^{2+}, Ga^{3+}, Ag^{+}, Cd^{2+}, and In^{3+}) as the third component into benzophenone (Fig. 10e).[121] The coordination between the guest molecules and the metal ions resulted in a comprehensive enhancement of phosphorescence properties, encompassing the phosphorescence efficiency, wavelength, and lifetime, in the doped materials (Fig. 10e). Both studies presented a straightforward, efficient, and universally applicable strategy for fine-tuning the phosphorescent characteristics of doped materials.

Summary and outlook

Numerous efforts have been devoted to suppress the non-radiative transitions and enhance the phosphorescence efficiency by creating ionic interactions. In this perspective, we first illustrated that utilizing ionic compounds as organic RTP materials offers several advantages: enhanced phosphorescence efficiency due to strong SOC facilitated by heavy atoms, increased rigidity in the molecular architecture which can reduce non-radiative decay, and the possibility for tunable emissions by varying the ionic components. Subsequently, we systematically explored the influence of various intermolecular interactions in ionic systems, including the ion–π interactions, electrostatic interactions, and coordinate interactions on the phosphorescence properties at ambient conditions. In summary, ionic compounds provide greater flexibility of their molecular design and control, contributing to the optimization of RTP.

For further developments in ion-regulated organic RTP materials, the following issues and challenges need to be considered. Firstly, we need to deeply understand the functions and roles of ionic interactions in the phosphorescence emission, to achieve effective manipulation of the RTP performance including the phosphorescence color, lifetime, and quantum yield. Secondly, compared to classical inorganic systems, the long luminescence lifetimes in the studied ionic systems are significantly shorter. Moreover, high-performance materials of simultaneously possessing both ultra-long phosphorescence lifetimes and high phosphorescence efficiency in ionic systems are rare, and need to be further enriched. Thirdly, the inherent rigidity of ionic crystals results in poor processability, which severely hinders their practical applications in flexible electronics. Thus, considerable attention needs to be paid to the development of amorphous ionic RTP materials for easy processing. Fourthly, most of the reported ionic RTP materials exhibit short absorption and emission wavelengths, which impede their utility *in vivo* applications due to the limited tissue penetrability. Developing ionic RTP materials with infrared or near-infrared phosphorescence emission will be crucial to extend their applications *in vivo*. Finally, introducing functional groups to develop stimuli-responsive ionic RTP materials will endow them with more functionalities and support much wider applications.

Author contributions

Prof. Zhengxu Cai and Dongpeng Yan conceived the project. Wenbo Dai and Yitian Jiang conducted the literature review. Wenbo Dai carried out the concepts, design, definition of intellectual content, and manuscript preparation. Prof. Zhengxu Cai and Dongpeng Yan revised and finalized the manuscript. All authors contributed to the final version of the manuscript.

Conflicts of interest

There are no conflicts to declare.

Acknowledgements

The authors acknowledge the National Key Research and Development Program of China (2018YFA0901800), The National Natural Scientific Foundation of China (Grant number: 22222501, 22175023), and the Natural Science Foundation of Beijing Municipality (2232022). This work was also supported by BIT Research and Innovation Promoting Project (Grant no. 2023YCXZ016).

Notes and references

1 W. Zhao, Z. He and B. Z. Tang, *Nat. Rev. Mater.*, 2020, **5**, 869–885.
2 S. Hirata, *Appl. Phys. Rev.*, 2022, **9**, 011304.
3 M. Fang, J. Yang and Z. Li, *Prog. Mater. Sci.*, 2022, **125**, 100914.
4 J. Gu, Z. Li and Q. Li, *Coord. Chem. Rev.*, 2023, **475**, 214872.
5 Y. Lei, W. Dai, J. Guan, S. Guo, F. Ren, Y. Zhou, J. Shi, B. Tong, Z. Cai, J. Zheng and Y. Dong, *Angew. Chem., Int. Ed.*, 2020, **59**, 16054–16060.
6 S. Guo, W. Dai, X. Chen, Y. Lei, J. Shi, B. Tong, Z. Cai and Y. Dong, *ACS Mater. Lett.*, 2021, **3**, 379–397.
7 N. Gan, X. Zou, Y. Zhang, L. Gu and Z. An, *Appl. Phys. Rev.*, 2023, **10**, 021313.
8 X. Wang, H. Shi, H. Ma, W. Ye, L. Song, J. Zan, X. Yao, X. Ou, G. Yang, Z. Zhao, M. Singh, C. Lin, H. Wang, W. Jia, Q. Wang, J. Zhi, C. Dong, X. Jiang, Y. Tang, X. Xie,

Y. Yang, J. Wang, Q. Chen, Y. Wang, H. Yang, G. Zhang, Z. An, X. Liu and W. Huang, *Nat. Photon.*, 2021, **15**, 187–192.
9 F. Li, M. Wang, S. Liu and Q. Zhao, *Chem. Sci.*, 2022, **13**, 2184–2201.
10 H. Sun and L. Zhu, *Aggregate*, 2022, **4**, e253.
11 Y. Zhang, W. Zhang, J. Xia, C. Xiong, G. Li, X. Li, P. Sun, J. Shi, B. Tong, Z. Cai and Y. Dong, *Angew. Chem., Int. Ed.*, 2023, **62**, e202314273.
12 G. Zhang, G. M. Palmer, M. W. Dewhirst and C. L. Fraser, *Nat. Mater.*, 2009, **8**, 747–751.
13 X. Zhen, Y. Tao, Z. An, P. Chen, C. Xu, R. Chen, W. Huang and K. Pu, *Adv. Mater.*, 2017, **29**, 1606665.
14 Q. Dang, Y. Jiang, J. Wang, J. Wang, Q. Zhang, M. Zhang, S. Luo, Y. Xie, K. Pu, Q. Li and Z. Li, *Adv. Mater.*, 2020, **32**, 2006752.
15 W. Dai, Y. Zhang, X. Wu, S. Guo, J. Ma, J. Shi, B. Tong, Z. Cai, H. Xie and Y. Dong, *CCS Chem.*, 2022, **4**, 2550–2559.
16 F. Xiao, H. Gao, Y. Lei, W. Dai, M. Liu, X. Zheng, Z. Cai, X. Huang, H. Wu and D. Ding, *Nat. Commun.*, 2022, **13**, 186.
17 Y. Zhao, J. Yang, C. Liang, Z. Wang, Y. Zhang, G. Li, J. Qu, X. Wang, Y. Zhang, P. Sun, J. Shi, B. Tong, H.-Y. Xie, Z. Cai and Y. Dong, *Angew. Chem., Int. Ed.*, 2023, e202317431.
18 Y. Si, Y. Zhao, W. Dai, S. Cui, P. Sun, J. Shi, B. Tong, Z. Cai and Y. Dong, *Chin. J. Chem.*, 2023, **41**, 1575–1582.
19 Y. Zhang, J. Li, J. Zhao, X. Li, Z. Wang, Y. Huang, H. Zhang, Q. Liu, Y. Lei and D. Ding, *Angew. Chem., Int. Ed.*, 2023, e202313890.
20 Q. Li and Z. Li, *Acc. Chem. Res.*, 2020, **53**, 962–973.
21 W. Shao and J. Kim, *Acc. Chem. Res.*, 2022, **55**, 1573–1585.
22 H. Shi, W. Yao, W. Ye, H. Ma, W. Huang and Z. An, *Acc. Chem. Res.*, 2022, **55**, 3445–3459.
23 L. Gu, X. Wang, M. Singh, H. Shi, H. Ma, Z. An and W. Huang, *J. Phys. Chem. Lett.*, 2020, **11**, 6191–6200.
24 Q. Peng, H. Ma and Z. Shuai, *Acc. Chem. Res.*, 2021, **54**, 940–949.
25 Z. Xu, Y. He, H. Shi and Z. An, *SmartMat*, 2023, **4**, e1139.
26 C. C. Kenry and B. Liu, *Nat. Commun.*, 2019, **10**, 2111.
27 J. Guo, C. Yang and Y. Zhao, *Acc. Chem. Res.*, 2022, **55**, 1160–1170.
28 S. Cai, X. Yao, H. Ma, H. Shi and Z. An, *Aggregate*, 2023, **4**, e320.
29 Y. Zhang, C. Xiong, W. Wang, W. Dai, Y. Ren, J. Xia, G. Li, J. Shi, B. Tong, X. Zheng, X. Shao, Z. Cai and Y. Dong, *Aggregate*, 2023, **4**, e310.
30 W. Z. Yuan, X. Y. Shen, H. Zhao, J. W. Y. Lam, L. Tang, P. Lu, C. Wang, Y. Liu, Z. Wang, Q. Zheng, J. Z. Sun, Y. Ma and B. Z. Tang, *J. Phys. Chem. C*, 2010, **114**, 6090–6099.
31 Y. Gong, G. Chen, Q. Peng, W. Z. Yuan, Y. Xie, S. Li, Y. Zhang and B. Z. Tang, *Adv. Mater.*, 2015, **27**, 6195–6201.
32 E. Hamzehpoor and D. F. Perepichka, *Angew. Chem., Int. Ed.*, 2020, **59**, 9977–9981.
33 S. Garain, S. S. N. Ansari, A. Kongasseri, B. C. Garain, S. K. Pati and S. J. George, *Chem. Sci.*, 2022, **13**, 10011–10019.
34 Z. An, C. Zheng, Y. Tao, R. Chen, H. Shi, T. Chen, Z. Wang, H. Li, R. Deng, X. Liu and W. Huang, *Nat. Mater.*, 2015, **14**, 685–690.
35 L. Gu, H. Shi, L. Bian, M. Gu, K. Ling, X. Wang, H. Ma, S. Cai, W. Ning, L. Fu, H. Wang, S. Wang, Y. Gao, W. Yao, F. Huo, Y. Tao, Z. An, X. Liu and W. Huang, *Nat. Photon.*, 2019, **13**, 406–411.
36 S. Li, L. Fu, X. Xiao, H. Geng, Q. Liao, Y. Liao and H. Fu, *Angew. Chem., Int. Ed.*, 2021, **60**, 18059–18064.
37 X. Ma, J. Wang and H. Tian, *Acc. Chem. Res.*, 2019, **52**, 738–748.
38 X. K. Ma and Y. Liu, *Acc. Chem. Res.*, 2021, **54**, 3403–3414.
39 G. Wu, F. Li, B. Tang and X. Zhang, *J. Am. Chem. Soc.*, 2022, **144**, 14962–14975.
40 H. Gao and X. Ma, *Aggregate*, 2021, **2**, 38.
41 Z. Huang, Z. He, B. Ding, H. Tian and X. Ma, *Nat. Commun.*, 2022, **13**, 7841.
42 B. Ding, X. Ma and H. Tian, *Acc. Mater. Res.*, 2023, **4**, 827–838.
43 Y. Lei, W. Dai, Y. Tian, J. Yang, P. Li, J. Shi, B. Tong, Z. Cai and Y. Dong, *J. Phys. Chem. Lett.*, 2019, **10**, 6019–6025.
44 Y. Wang, J. Yang, Y. Gong, M. Fang, Z. Li and B. Z. Tang, *SmartMat*, 2020, **1**, 1006.
45 W. Dai, T. Bianconi, E. Ferraguzzi, X. Wu, Y. Lei, J. Shi, B. Tong, B. Carlotti, Z. Cai and Y. Dong, *ACS Mater. Lett.*, 2021, **3**, 1767–1777.
46 C. Chen, Z. Chi, K. C. Chong, A. S. Batsanov, Z. Yang, Z. Mao, Z. Yang and B. Liu, *Nat. Mater.*, 2021, **20**, 175–180.
47 X. Chen, W. Dai, X. Wu, H. Su, C. Chao, Y. Lei, J. Shi, B. Tong, Z. Cai and Y. Dong, *Chem. Eng. J.*, 2021, **426**, 131607.
48 W. Dai, X. Niu, X. Wu, Y. Ren, Y. Zhang, G. Li, H. Su, Y. Lei, J. Xiao, J. Shi, B. Tong, Z. Cai and Y. Dong, *Angew. Chem., Int. Ed.*, 2022, **61**, e202200236.
49 X. Yan, H. Peng, Y. Xiang, J. Wang, L. Yu, Y. Tao, H. Li, W. Huang and R. Chen, *Small*, 2022, **18**, e2104073.
50 G. Li, W. Dai, Y. Lei, J. Shi, B. Tong, Z. Cai and Y. Dong, *ChemPhotoChem*, 2022, **7**, e202200198.
51 Y. Ren, W. Dai, S. Guo, L. Dong, S. Huang, J. Shi, B. Tong, N. Hao, L. Li, Z. Cai and Y. Dong, *J. Am. Chem. Soc.*, 2022, **144**, 1361–1369.
52 Y. Lei, W. Dai, G. Li, Y. Zhang, X. Huang, Z. Cai and Y. Dong, *J. Phys. Chem. Lett.*, 2023, **14**, 1794–1807.
53 B. Wang, Z. Sun, J. Yu, G. I. N. Waterhouse, S. Lu and B. Yang, *SmartMat*, 2022, **3**, 337–348.
54 K. Wang, L. Qu and C. Yang, *Small*, 2023, **19**, e2206429.
55 E. Hamzehpoor, C. Ruchlin, Y. Tao, C. H. Liu, H. M. Titi and D. F. Perepichka, *Nat. Chem.*, 2023, **15**, 83–90.
56 X. Liang, X.-F. Luo, Z.-P. Yan, Y.-X. Zheng and J.-L. Zuo, *Angew. Chem., Int. Ed.*, 2021, **60**, 24437–24442.
57 X. Xu, Z. Chen, Y. Lei, X. Sun, M. Liu, H. Wu and X. Huang, *Chem. Commun.*, 2022, **58**, 11143–11146.
58 I. Partanen, O. Al-Saedy, T. Eskelinen, A. J. Karttunen, J. J. Saarinen, O. Mrozek, A. Steffen, A. Belyaev, P. T. Chou and I. O. Koshevoy, *Angew. Chem., Int. Ed.*, 2023, **62**, e202305108.
59 F. Nie, B. Zhou and D. Yan, *Chem. Eng. J.*, 2023, **453**, 139806.
60 Y. Liu, Y. Ma, X. Fang, T. Chen, F. Nie and D. Yan, *J. Mater. Chem. C*, 2023, **11**, 15855–15860.
61 P. She, Y. Yu, Y. Qin, Y. Zhang, F. Li, Y. Ma, S. Liu, W. Huang and Q. Zhao, *Adv. Opt. Mater.*, 2019, **8**, 1901437.

62 S. Liu, Y. Lin and D. Yan, *Sci. Bull.*, 2022, **67**, 2076–2084.
63 J. Wei, M. Zhu, T. Du, J. Li, P. Dai, C. Liu, J. Duan, S. Liu, X. Zhou, S. Zhang, L. Guo, H. Wang, Y. Ma, W. Huang and Q. Zhao, *Nat. Commun.*, 2023, **14**, 4839.
64 S. Liu, X. Fang, B. Lu and D. Yan, *Nat. Commun.*, 2020, **11**, 4649.
65 B. Zhou, G. Xiao and D. Yan, *Adv. Mater.*, 2021, **33**, e2007571.
66 G. Xiao, X. Fang, Y. J. Ma and D. Yan, *Adv. Sci.*, 2022, **9**, e2200992.
67 O. Pajuelo-Corral, A. Rodríguez-Diéguez, G. Beobide, S. Pérez-Yáñez, J. A. García, E. San Sebastian, J. M. Seco and J. Cepeda, *J. Mater. Chem. C*, 2019, **7**, 6997–7012.
68 L. J. Xu, A. Plaviak, X. Lin, M. Worku, Q. He, M. Chaaban, B. J. Kim and B. Ma, *Angew. Chem., Int. Ed.*, 2020, **59**, 23067–23071.
69 S. Feng, Y. Ma, S. Wang, S. Gao, Q. Huang, H. Zhen, D. Yan, Q. Ling and Z. Lin, *Angew. Chem., Int. Ed.*, 2022, e202116511.
70 R. Gao, M. S. Kodaimati and D. Yan, *Chem. Soc. Rev.*, 2021, **50**, 5564–5589.
71 Z. Qi, B. Zhou and D. Yan, *Mater. Chem. Front.*, 2023, **7**, 3475–3493.
72 B. Zhou and D. Yan, *Adv. Funct. Mater.*, 2023, **33**, 2300735.
73 X. Li, Y. Wang, Z. Zhang, S. Cai, Z. An and W. Huang, *Adv. Mater.*, 2023, e2308290.
74 W. Ye, H. Ma, H. Shi, H. Wang, A. Lv, L. Bian, M. Zhang, C. Ma, K. Ling, M. Gu, Y. Mao, X. Yao, C. Gao, K. Shen, W. Jia, J. Zhi, S. Cai, Z. Song, J. Li, Y. Zhang, S. Lu, K. Liu, C. Dong, Q. Wang, Y. Zhou, W. Yao, Y. Zhang, H. Zhang, Z. Zhang, X. Hang, Z. An, X. Liu and W. Huang, *Nat. Mater.*, 2021, **20**, 1539–1544.
75 L. Xiao and H. Fu, *Chem.–Eur. J.*, 2019, **25**, 714–723.
76 F. Xiao, M. Wang, Y. Lei, W. Dai, Y. Zhou, M. Liu, W. Gao, X. Huang and H. Wu, *J. Mater. Chem. C*, 2020, **8**, 17410–17416.
77 N. Liu, Y. Pan, Y. Lei, M. Liu, C. Peng, Z. Cai, G. Shen, H. Wu, X. Huang and Y. Dong, *Chem. Eng. J.*, 2022, **433**, 133530.
78 J. Wang, X. Gu, P. Zhang, X. Huang, X. Zheng, M. Chen, H. Feng, R. T. K. Kwok, J. W. Y. Lam and B. Z. Tang, *J. Am. Chem. Soc.*, 2017, **139**, 16974–16979.
79 G. Jiang, J. Yu, J. Wang and B. Z. Tang, *Aggregate*, 2022, **3**, e285.
80 J. Wang, X. Gu, H. Ma, Q. Peng, X. Huang, X. Zheng, S. H. P. Sung, G. Shan, J. W. Y. Lam, Z. Shuai and B. Z. Tang, *Nat. Commun.*, 2018, **9**, 2963.
81 X. Chen, C. Xu, T. Wang, C. Zhou, J. Du, Z. Wang, H. Xu, T. Xie, G. Bi, J. Jiang, X. Zhang, J. N. Demas, C. O. Trindle, Y. Luo and G. Zhang, *Angew. Chem., Int. Ed.*, 2016, **55**, 9872–9876.
82 Z. Yang, Z. Mao, X. Zhang, D. Ou, Y. Mu, Y. Zhang, C. Zhao, S. Liu, Z. Chi, J. Xu, Y.-C. Wu, P.-Y. Lu, A. Lien and M. R. Bryce, *Angew. Chem., Int. Ed.*, 2016, **55**, 2181–2185.
83 A. Cheng, H. Su, X. Gu, W. Zhang, B. Zhang, M. Zhou, J. Jiang, X. Zhang and G. Zhang, *Angew. Chem., Int. Ed.*, 2023, **62**, e202312627.
84 S. Garain, S. M. Wagalgave, A. A. Kongasseri, B. C. Garain, S. N. Ansari, G. Sardar, D. Kabra, S. K. Pati and S. J. George, *J. Am. Chem. Soc.*, 2022, **144**, 10854–10861.
85 P. Yu, Y. Zhen, H. Dong and W. Hu, *Chem*, 2019, **5**, 2814–2853.
86 Z. Cheng, H. Shi, H. Ma, L. Bian, Q. Wu, L. Gu, S. Cai, X. Wang, W. W. Xiong, Z. An and W. Huang, *Angew. Chem., Int. Ed.*, 2018, **57**, 678–682.
87 G. Chen, H. Feng, F. Feng, P. Xu, J. Xu, S. Pan and Z. Qian, *J. Phys. Chem. Lett.*, 2018, **9**, 6305–6311.
88 G. Chen, S. Guo, H. Feng and Z. Qian, *J. Mater. Chem. C*, 2019, **7**, 14535–14542.
89 G. Xiao, Y. J. Ma, X. Fang and D. Yan, *ACS Appl. Mater. Interfaces*, 2022, **14**, 30246–30255.
90 W. Chen, Z. Tian, Y. Li, Y. Jiang, M. Liu and P. Duan, *Chem.–Eur. J.*, 2018, **24**, 17444–17448.
91 S. Feng, Q. Huang, S. Yang, Z. Lin and Q. Ling, *Chem. Sci.*, 2021, **12**, 14451–14458.
92 D. Braga, F. Grepioni and G. R. Desiraju, *Chem. Rev.*, 1998, **98**, 1375–1406.
93 Y. Zhang, Y. Su, H. Wu, Z. Wang, C. Wang, Y. Zheng, X. Zheng, L. Gao, Q. Zhou, Y. Yang, X. Chen, C. Yang and Y. Zhao, *J. Am. Chem. Soc.*, 2021, **143**, 13675–13685.
94 S. Z. Cai, H. L. Ma, H. F. Shi, H. Wang, X. Wang, L. X. Xiao, W. P. Ye, K. W. Huang, X. D. Cao, N. Gan, C. Q. Ma, M. X. Gu, L. L. Song, H. Xu, Y. T. Tao, C. F. Zhang, W. Yao, Z. F. An and W. Huang, *Nat. Commun.*, 2019, **10**, 4247.
95 H. Wang, H. Shi, W. Ye, X. Yao, Q. Wang, C. Dong, W. Jia, H. Ma, S. Cai, K. Huang, L. Fu, Y. Zhang, J. Zhi, L. Gu, Y. Zhao, Z. An and W. Huang, *Angew. Chem., Int. Ed.*, 2019, **58**, 18776–18782.
96 B. Zhao, S. Yang, X. Yong and J. Deng, *ACS Appl. Mater. Interfaces*, 2021, **13**, 59320–59328.
97 S. Tang, T. Yang, Z. Zhao, T. Zhu, Q. Zhang, W. Hou and W. Z. Yuan, *Chem. Soc. Rev.*, 2021, **50**, 12616–12655.
98 T. Zhu, T. Yang, Q. Zhang and W. Z. Yuan, *Nat. Commun.*, 2022, **13**, 2658.
99 S. Tang, Z. Zhao, J. Chen, T. Yang, Y. Wang, X. Chen, M. Lv and W. Z. Yuan, *Angew. Chem., Int. Ed.*, 2022, **61**, e202117368.
100 J. Zhang, P. Alam, S. Zhang, H. Shen, L. Hu, H. H. Y. Sung, I. D. Williams, J. Sun, J. W. Y. Lam, H. Zhang and B. Z. Tang, *Nat. Commun.*, 2022, **13**, 3492.
101 X. Luo, B. Tian, Y. Zhai, H. Guo, S. Liu, J. Li, S. Li, T. D. James and Z. Chen, *Nat. Rev. Chem*, 2023, **7**, 800–812.
102 Z. Zhu, L. Zeng, W. Li, W. Xu and D. Tian, *ACS Sustain. Chem. Eng.*, 2022, **10**, 16752–16759.
103 X. Zhang, Y. Cheng, J. You, J. Zhang, C. Yin and J. Zhang, *Nat. Commun.*, 2022, **13**, 1117.
104 J. You, X. Zhang, Q. Nan, K. Jin, J. Zhang, Y. Wang, C. Yin, Z. Yang and J. Zhang, *Nat. Commun.*, 2023, **14**, 4163.
105 Y. Zhai, S. Li, J. Li, S. Liu, T. D. James, J. L. Sessler and Z. Chen, *Nat. Commun.*, 2023, **14**, 2614.
106 L. Zeng, Z. Zhu, R. Mo, W. Li, W. Xu and D. Tian, *Chem. Eng. J.*, 2023, **460**, 141452.
107 Z.-A. Yan, X. Lin, S. Sun, X. Ma and H. Tian, *Angew. Chem., Int. Ed.*, 2021, **60**, 19735–19739.

108 Z. Wang, A. Li, Z. Zhao, T. Zhu, Q. Zhang, Y. Zhang, Y. Tan and W. Z. Yuan, *Adv. Mater.*, 2022, **34**, e2202182.
109 A. Winter and U. S. Schubert, *Chem. Soc. Rev.*, 2016, **45**, 5311–5357.
110 Y. J. Ma, Z. Qi, G. Xiao, X. Fang and D. Yan, *Inorg. Chem.*, 2022, **61**, 16477–16483.
111 H. Liu, K. Zhang, P. F. Gao, J. H. Luo, Y. Y. Jiang, M. S. Zhou, T. Li, X. L. Zhu and H. R. Fu, *Inorg. Chem.*, 2022, **61**, 1636–1643.
112 X. Yang and D. Yan, *Adv. Opt. Mater.*, 2016, **4**, 897–905.
113 X. Yang and D. Yan, *Chem. Sci.*, 2016, **7**, 4519–4526.
114 F. Nie, K. Z. Wang and D. Yan, *Nat. Commun.*, 2023, **14**, 1654.
115 B. Zhou, Z. Qi and D. Yan, *Angew. Chem., Int. Ed.*, 2022, **61**, e202208735.
116 A. Kishimura, T. Yamashita, K. Yamaguchi and T. Aida, *Nat. Mater.*, 2005, **4**, 546–549.
117 H. Sun, S. Liu, W. Lin, K. Y. Zhang, W. Lv, X. Huang, F. Huo, H. Yang, G. Jenkins, Q. Zhao and W. Huang, *Nat. Commun.*, 2014, **5**, 3601.
118 C. H. Li, C. Wang, C. Keplinger, J. L. Zuo, L. Jin, Y. Sun, P. Zheng, Y. Cao, F. Lissel, C. Linder, X. Z. You and Z. Bao, *Nat. Chem.*, 2016, **8**, 618–624.
119 P. Wei, J. Liu, G. G. Shan, X. Zhang, H. Zhang, J. Qi, W. Zhao, H. H. Sung, I. D. Williams, J. W. Y. Lam and B. Z. Tang, *Angew. Chem., Int. Ed.*, 2019, **59**, 9293–9298.
120 W. Dai, G. Li, Y. Zhang, Y. Ren, Y. Lei, J. Shi, B. Tong, Z. Cai and Y. Dong, *Adv. Funct. Mater.*, 2023, **33**, 2210102.
121 Y. Guo, K. Chen, Z. Hu, Y. Lei, X. Liu, M. Liu, Z. Cai, J. Xiao, H. Wu and X. Huang, *J. Phys. Chem. Lett.*, 2022, **13**, 7607–7617.